J|A|C|S COMMUNICATIONS

Published on Web 08/04/2010

Diffusion of Metal in a Confined Nanospace of Carbon Nanotubes Induced by Air Oxidation

Jisheng Zhou, Huaihe Song,* Xiaohong Chen, and Junping Huo

State Key Laboratory of Chemical Resource Engineering, Beijing University of Chemical Technology, Beijing 100029, P. R. China

Received June 29, 2010; E-mail: songhh@mail.buct.edu.cn

Abstract: Air oxidation can result in the motion of metal confined in carbon nanotubes (CNTs). This can also be utilized to tailor various hybrid nanostructures. By controllable air-oxidation, as-prepared metal@CNT nanorods (a) can be converted first to core−shell−void nanorods (b), then to metal/metal oxide@CNT nanotubes (c), and finally to mesoporous metal oxide nanotubes (d). The metal/metal oxide@CNT nanotubes and mesoporous metal oxide nanotubes are expected to find many applications, such as in lithium ion batteries, catalysis, magnetic drug delivery, and gas sensing.

Carbon nanotubes (CNTs) filled with metals[1] have gained extensive attention because of their potential applications in data storage, catalysis, and electronic devices. The interaction of interior materials with CNTs[2] has attracted intensive interest for the further exploration of novel physicochemical phenomena as well as for the design of emerging nano-objects by using the confinement of CNTs. Recent simulations[3] and experiments[4−6] strongly indicate that metal confined within the one-dimensional (1D) nanospace of CNTs can be driven to migrate by external stimuli such as high-energy electron beam irradiation (HEEBI),[4,7] voltage gradients,[5] and stepwise current.[6] To date, on one hand, interior metal can move/diffuse along the CNTs, with the CNTs acting as a pipeline of mass transport, while on the other hand, metal can also be incorporated into the interlayers and/or vacancies of CNTs to form a hybrid shell by HEEBI.[5] Generally, these processes, especially the incorporation of metal into the carbon layers of CNTs, need a high energy, so it is very difficult for them to occur by thermal activation.[2] Here we demonstrate that thermal air oxidation to activate the surface of CNTs can also manipulate the migration of interior metal atoms. The strategy is motivated by the so-called nanoscale Kirkendall effect, which can effectively induce the outward diffusion of atoms in metal nanoparticles/nanowires to form hollow nanostructures by oxidation.[8] It is very interesting to consider whether metal atoms in a 1D confined nanospace of a CNT can also sense the oxidation atmosphere outside the CNT. However, the case has never been investigated, because conventional attention has been focused on the ability of CNTs to protect encapsulated materials against environmental attack.[1]

Scheme 1

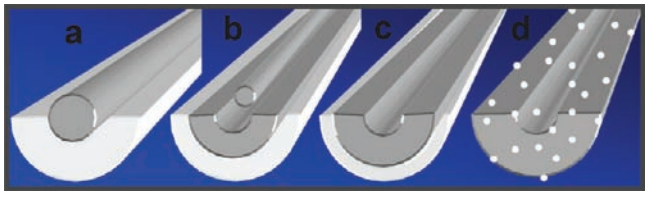

Scheme 1 illustrates the diffusion process of metal in the confined nanospace of a CNT. By controllable air oxidation, metal@CNT nanorods (a) can be converted first to core−shell−void nanorods (b), then to metal/metal oxide@CNT nanotubes (c), and finally to mesoporous metal oxide nanotubes (d). Thus, one can not only investigate the oxidation-induced diffusion behavior and mechanism of metal atoms in CNTs but also design various novel hybrid nanostructures that will also be of scientific and technological importance to both CNTs and metal nanostructures. Our recent advances in fabrication and conversion of CNT-encapsulated metal nanowires/rods and carbon-encapsulated metal nanoparticles[9] allow the rational design of hybrid nanotubes based on this approach. Subsequently, the conversion process of Fe_3C@CNT nanorods as a special example displays this strategy in detail. This fundamental strategy should also be applicable to the preparation of a broad range of nanostructures depending on the components of the selected metal core in CNT-encapsulated metal nanowires/rods.

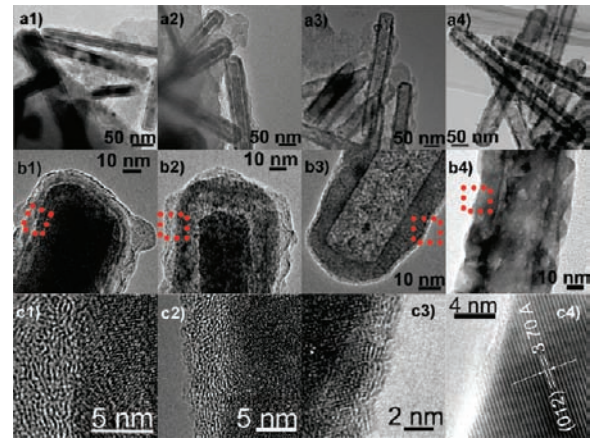

Figure 1. (a1−4) Bright-field TEM images of sample A (original Fe_3C@CNT nanorods), sample B (obtained by air oxidation at 240 °C), sample C (obtained at 280 °C), and sample D (the final Fe_2O_3 nanotubes obtained at 350 °C for 24 h), respectively. (b1−4) TEM images of single nanostructures for samples A−D, respectively. (c1−4) Enlarged HRTEM images of the selected areas in b1−4, respectively.

Fe_3C@CNT nanorods (sample A, Figure 1a1) were prepared in our pervious work.[9] Their length, outer diameter, and shell thickness are in the ranges 150−350, 30−50, and 5−8 nm, respectively. The X-ray diffraction (XRD) pattern (Figure S1 in the Supporting Information) shows that the core material is Fe_3C. Ion-etching X-ray photoelectron spectroscopy (XPS) depth-profiling analysis (Figure S2) indicates that no iron is detected in the carbon shells. Figure 1b1 shows a representative Fe_3C@CNT nanorod. High-resolution transmission electron microscopy (HRTEM) images (Figure 1c1 and Figure S3b) show the semigraphitic structure of the carbon shells, while the core is polycrystalline Fe_3C. The detailed elemental

10.1021/ja105712w

distribution of the nanorod was investigated by high-angle annular dark-field (HAADF) scanning transmission electron microscopy (STEM) and energy-dispersive X-ray (EDX) elemental mapping and line-scan profile. Figure 2a1−f1 clearly demonstrates that iron in sample A was detected strongly in the core region and away from the shell region, whereas carbon was located in both the core and shell regions and no oxygen is detected (Figure S3). These results indicate that the core consisted of Fe/C compound and was coated by a carbon shell, which is in good agreement with previous reports.[10]

The metal core in sample A can diffuse outward to form various nanostructures by air oxidation from room temperature to the designed temperature. An interesting "core−void−shell" nanostructure (sample B, Figure 1a2) with a gap between the core and shell was obtained when the temperature was increased to 240 °C. In comparison with sample A, the shell thickness increased to 11−14 nm and the core shrank to 15−30 nm for sample B; Fe_3C was still the dominating core component, although Fe_3O_4 was present after oxidation (Figure S1). The individual core−void−shell nanorod shown in Figure 1b2 is analyzed in detail. The clear bright/dark contrast shows that the shell consists of two layers. The HRTEM image confirms the presence of multicrystalline iron compounds in the inner layer and the semigraphitic carbon layer in the outer one (Figure 1c2), indicating that iron migrates from the core into the shell. Furthermore, the HAADF-STEM image (Figure 2a2), elemental mapping (Figure 2c2), and line-scan profile (Figure 2f2) also clearly exhibit the same results. Simultaneously, elemental mappings also show that the remaining core is still an Fe/C compound. Noticeably, no oxygen element in the chosen nanorods was detected by EDX analysis (Figure 2d2 and Figure S4), suggesting that no iron was oxidized. On the basis of this and the XRD results, iron in both the core and shell regions should exist in the form of Fe_3C, which was further confirmed in the subsequent analysis.

It is very interesting to consider how the core materials diffuse outward, because this process involves not only iron but also carbon located in the core region. The outward diffusions of carbon and iron exhibit similar tendencies, as shown by a comparison of the change in the spatial elemental distribution from sample A to B; this indicates that the carbon in the core should diffuse outward together with the iron. More interestingly, an HRTEM image (Figure 3) reveals the continuous lattice fringes from the core to the shell, which can be assigned to the (121) plane of Fe_3C. This provides direct evidence that core materials diffuse outward in the form of Fe_3C and confirms again that the iron that diffuses into the shell exists mainly in the form of Fe_3C, consistent with the deduction above. The remaining cores in sample B are rougher than those of sample A, which may be attributed to the various diffusion rates of Fe_3C at different lattice planes. We emphasize that the diffusion in our case is obviously different from the surface diffusion during the Kirkendall process reported by Fan et al.[8b]

The core disappeared completely to form a hollow interior when the oxidation temperature was increased. At 280 °C, nanotubes were formed (sample C, Figure 1a3). The microstructure and spatial elemental distribution of a typical nanotube also show its tubular nanostructure (Figures 1b3 and 2a3−f3). The shell of sample C also consists of two layers (Figure 1c2). The outer layer is still a carbon layer (Figure 1c3). Furthermore, carbon elemental mapping (Figure 2b2) also revealed that carbon in the shell region can be divided into two parts. The outer highlight part should be attributed to the carbon layer shown in Figure 1c3. The inner part shows a distribution similar to those of iron and oxygen. Therefore, the inner layer is composed of C, Fe, and O. Quantitative EDX analysis

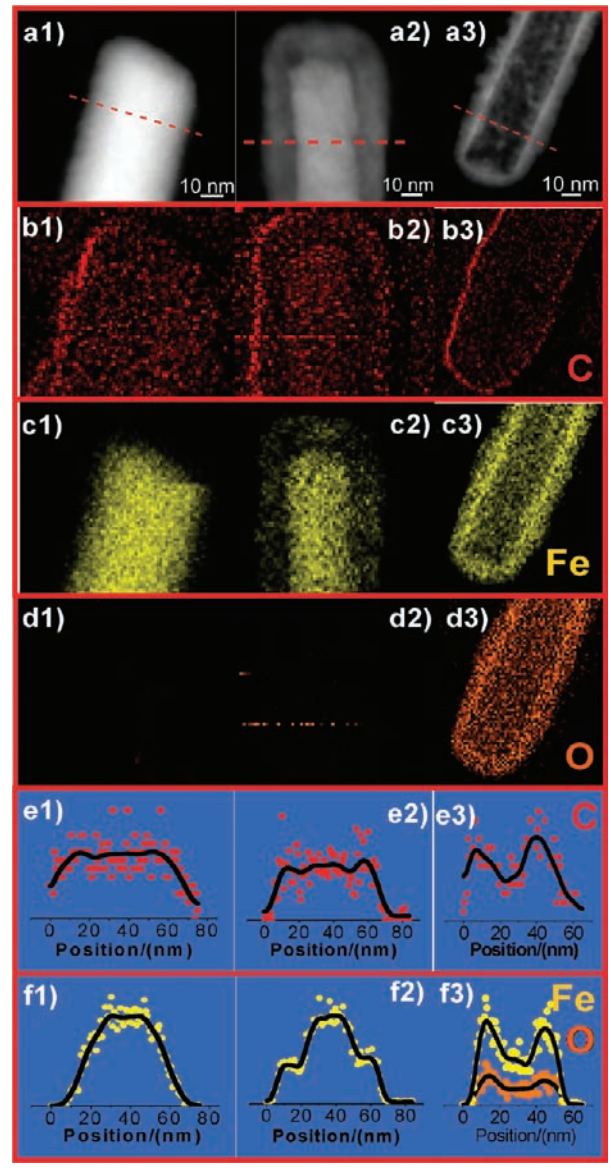

Figure 2. (a1−3) HAADF images of samples A−C. (b−d) Corresponding elemental maps of (b1−3) C, (c1−3) Fe, and (d1−3) O. (e, f) EDX line-scan profiles for (e1−3) C and (f1−3) Fe (yellow) and O (red) along the red lines in a1−3, respectively.

showed an O/Fe atomic ratio of 0.9:1, which is lower than the stoichiometric ratio in Fe_3O_4 (Figure S5). The line-scan profiles (Figure 2f) also showed that the signal intensity of O through the shell is lower than that of Fe. These results imply that unoxidized Fe exists in the shell. It is further confirmed that the iron in sample C is still assigned to dominant Fe_3C and partial Fe_3O_4 (Figure S1). HRTEM observation confirmed the presence of Fe_3C in the inner shell (Figure S3), consistent with above analysis of sample B. The XPS depth analysis also indicated that iron exists mainly in the form of iron oxide in the outer shell of sample C and as Fe_3C in the inner shell. Therefore, sample C consists of Fe_3C/Fe_3O_4@CNT hybrid nanotubes.

CNTs can be obtained by completely removing the metal in sample C using HCl (Figure S6), and the mixing region of carbon layers and metal lattice planes in the shells can also be observed by the careful HRTEM analysis (Figure S5). These results indicate that the Fe atoms diffusing into the shell are embedded in vacancies and/or interstices of the CNTs. Surprisingly, statistical EDX analysis (Figure S7) showed that C/Fe atomic ratios in samples A−C are

almost the same, implying that carbon is not consumed in going from A to C and that the motion of the Fe atoms is confined only to the 1D nanospace of the CNTs. In addition, the thickness of the carbon layers in the outer part of the shells decreases in going from sample A to C, indicating that Fe atoms in the shells can continue to diffuse out along the carbon layers. Furthermore, sample C is converted to iron oxide@CNT nanotubes rather than pure CNTs by further oxidation (Figure S8), indicating the inward diffusion of oxygen through the carbon layers and showing that the CNT shells are the reaction interface of iron and oxygen. Eventually, porous α-Fe_2O_3 nanotubes with high crystallinity are formed by completely exhausting the carbon (Figure 1a4−c4 and Figures S9 and S10).

One important point requiring clarification is what factors (oxygen, heat treatment, or others) lead to the outward diffusion of the core materials. Annealing alone at 280 °C in a nitrogen flow does not result in the formation of hollow nanostructures, so it is reasonable to believe that oxygen is a driving force for their motion and that heating can help to accelerate this outward diffusion of the interior core.[9c] At the initial oxidation stage, although no oxygen was detected in the nanorod shown in Figure 1b2, the diffusion actually happens, implying that a physical process occurs in this stage. With the increase in heating temperature, the appearance of metal oxide accompanies the evolution of the hollow nanostructure, suggesting the combined action of physical and chemical processes. Obviously, our observations are different from previous reports,[7] in which the outward diffusion of metals (Cu, Co, Au, and Ni) into carbon layers is driven by the high-energy electron beam, which is a physical method. The detailed mechanism needs to be investigated further.

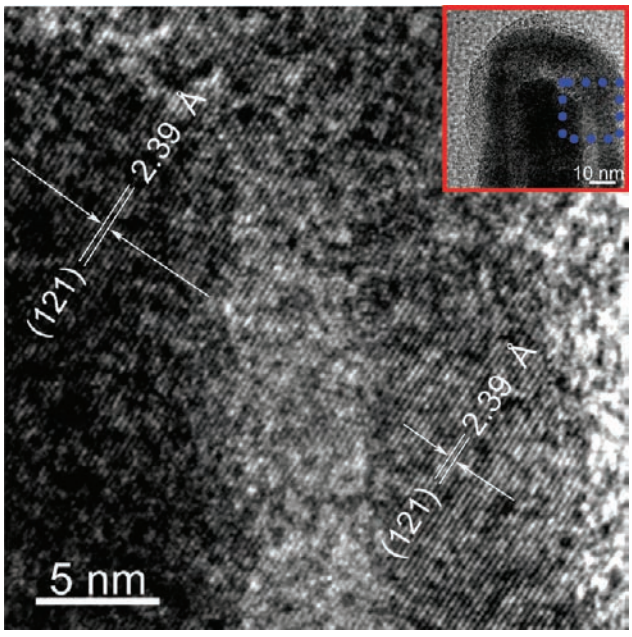

Figure 3. Megascopic HRTEM image of sample B corresponding to the selected blue area in the inset image.

The diffusion of metal confined in CNTs is also different from that of metal without CNT coating. In our samples, the outer diameter stayed constant from sample A to C, and unoxidized Fe_3C appeared in the inner shell of sample C. However, in a general way, the diameter of hollow nanostructures obtained from bare metal without a CNT coating is larger than the original diameter, and there is no unoxidized metal in the shells to be detected,[8] although oxide shells are frequently present (such as initial amorphous oxide on the metal nanoparticles[8a] or Al_2O_3 shells on ZnO nanowires[8b]) during the Kirkendall process. This indicates the special function of the CNT shell, which differs from the oxide shell in previous reports.[8] Carbon layers in CNTs acting as reaction interfaces for oxygen and iron species can directly control their interdiffusion.[9b,c] Thus, it is more facile to tailor nanostructures with various structures and components. Apparently, the crystallization degree of the CNT also has a great influence on the motion behavior of the metal core. The semigraphitic CNTs, containing many defects and vacancies, can provide efficient channels for outward migration of iron atoms and enhance the formation of hollow nanostructures.

Finally, we note that formation of a hollow interior is also related to the encapsulated materials. Qiu and co-workers[11] have reported that CNT-encapsulated CeF_3 nanowires are transformed into pure CeF_3 nanowires rather than oxide nanotubes by air oxidation, which may be attributed to the fact that the reaction of CeF_3 with oxygen is very difficult. In contrast, the reaction of Fe_3C with oxygen occurs prior to that of oxygen with carbon, so iron atoms must move outward to combine with oxygen atoms. Other CNT-encapsulated metals that are apt to react with oxygen, such as Co, can also form oxide nanotubes (Figure S11), indicating that this approach should be a general route for the bulk synthesis of metal/metal oxide@CNTs and metal oxide nanotubes. Metal−CNT interactions depend strongly on the type of metal.[12] Therefore, there should be variation in the behavior of the outward motion for different types of metal in the CNTs, which needs to be further investigated.

In summary, air oxidation can result in the motion of metal atoms confined in CNTs. This can also be utilized to tailor various hybrid nanostructures, such as core−void−shell nanorods, metal/metal oxide@CNT nanotubes, and porous metal oxide nanotubes. These novel hybrid nanostructures are expected to be applied in lithium ion batteries, magnetic drug delivery, and microwave absorption materials because of the outer carbon layers with high electronic conductivity and biocompatibility. As a preliminary test, iron oxide@CNT nanotubes used as anode materials for lithium ion batteries exhibited a high reversible capacity of 878 mA h g^{-1} and high-rate performance (Figure S12).

Acknowledgment. This work was supported by the National Natural Science Foundation of China (50572003 and 50972004), the State Key Basic Research Program of China (2006CB9326022006), and the Foundation of Excellent Doctoral Dissertation of Beijing City (YB20081001001).

Supporting Information Available: Descriptions of HRTEM, XPS, XRD, and EDX measurements and analysis. This material is available free of charge via the Internet at http://pubs.acs.org.

References

(1) (a) Ajayan, P. M.; Iijima, S. *Nature* **1993**, *361*, 333. (b) Guerret-Plécourt, C.; Bouar, Y. L.; Loiseau, A.; Pascard, H. *Nature* **1994**, *372*, 761. (c) Guan, L.; Suenaga, K.; Okubo, S.; Okazaki, T.; Iijima, S. *J. Am. Chem. Soc.* **2008**, *130*, 2162. (d) Kitaura, R.; Imazu, N.; Kobayashi, K.; Shinohara, H. *Nano Lett.* **2006**, *8*, 693. (e) Kitaura, R.; Nakanishi, R.; Satio, T.; Yoshikawa, H.; Awaga, K.; Shinohara, H. *Angew. Chem., Int. Ed.* **2009**, *48*, 8298.
(2) Banhart, F. *Nanoscale* **2009**, *1*, 201.
(3) (a) Schoen, P. A. E.; Walther, J. H.; Arcidiacono, S.; Poulikakos, D.; Koumoutsakos, P. *Nano Lett.* **2006**, *6*, 1910. (b) Schoen, P. A. E.; Walther, J. H.; Poulikakos, D.; Koumoutsakos, P. *Appl. Phys. Lett.* **2007**, *90*, 253116.
(4) (a) Sun, L.; Banhart, F.; Krasheninnikov, A. V.; Rodríguez-Manzo, J. A.; Terrones, M.; Ajayan, P. M. *Science* **2006**, *312*, 1199. (b) Warner, J. H.; Ito, Y.; Rümmeli, M. H.; Gemming, T.; Büchner, B.; Shinohara, H.; Briggs, G. A. D. *Phys. Rev. Lett.* **2009**, *102*, 195504. (c) Warner, J. H.; Ito, Y.; Rüchner, B.; Shinohara, H.; Briggs, G. A. D. *ACS Nano* **2009**, *3*, 3037.
(5) (a) Regan, B. C.; Aloni, S.; Ritchie, R. O.; Dahmen, U.; Zettl, A. *Nature* **2004**, *428*, 924. (b) Golberg, D.; Costa, P. M. F.; Mitome, M.; Hampel, S.; Haase, D.; Mueller, C.; Leonhardt, A.; Bando, Y. *Adv. Mater.* **2007**, *19*, 1937. (c) Dong, L.; Tao, X.; Zhang, L.; Zhang, X.; Nelson, B. J. *Nano Lett.* **2007**, *7*, 58.

(6) (a) Costa, P. M. F. J.; Golberg, D.; Mitome, M.; Hampel, S.; Leonhardt, A.; Buchner, B.; Bando, Y. *Nano Lett.* **2008**, *8*, 3120. (b) Dong, L.; Tao, X.; Hamadi, M.; Zhang, L.; Zhang, X.; Ferreira, A.; Nelson, B. J. *Nano Lett.* **2009**, *9*, 210.
(7) (a) Schaper, A. K.; Hou, H.; Greiner, A.; Schneider, R.; Phillipp, F. *Appl. Phys. A: Mater. Sci. Process.* **2004**, *78*, 73. (b) Banhar, F.; Charlier, J.-C.; Ajayan, P. M. *Phys. Rev. Lett.* **2000**, *84*, 686. (c) Banhart, F.; Redlich, P.; Ajayan, P. M. *Chem. Phys. Lett.* **1998**, *292*, 554.
(8) (a) Yin, Y.; Rioux, R. M.; Erdonmez, C. K.; Hughes, S.; Somorjai, G. A.; Alivisatos, A. P. *Science* **2004**, *304*, 711. (b) Fan, H. J.; Knez, M.; Scholz, R.; Nielsch, K.; Pippel, E.; Hesse, D.; Zacharias, M.; Gösele, U. *Nat. Mater.* **2006**, *5*, 627.
(9) (a) Huo, J.; Song, H.; Chen, X.; Lian, W. *Carbon* **2006**, *44*, 2849. (b) Zhou, J.; Song, H.; Chen, X.; Zhi, L.; Yang, S.; Huo, J.; Yang, W. *Chem. Mater.* **2009**, *21*, 2935. (c) Zhou, J.; Song, H.; Chen, X.; Zhi, L.; Huo, J.; Cheng, B. *Chem. Mater.* **2009**, *21*, 3730.
(10) (a) Tao, F.; Liang, Y.; Yin, G.; Xu, D.; Jiang, Z.; Lin, H.; Han, M.; Song, Y.; Xie, Z.; Xue, Z.; Zhu, J.; Xu, Z.; Zheng, L.; Wei, X.; Ni, Y. *Adv. Funct. Mater.* **2007**, *17*, 1124. (b) Jung, Y.; Lee, S.-H.; Jennings, A. T.; Agarwal, R. *Nano Lett.* **2008**, *8*, 2056.
(11) Wang, Z.; Zhao, Z.; Qiu, J. *Chem. Mater.* **2007**, *19*, 3364.
(12) (a) Zhang, Y.; Franklin, N. M.; Chen, R. J.; Dai, H. *Chem. Phys. Lett.* **2000**, *331*, 35. (b) Maiti, A.; Ricca, A. *Chem. Phys. Lett.* **2004**, *395*, 7.

JA105712W